Prediction of high-T_c superconductivity in ternary actinium beryllium hydrides at low pressure

Kun Gao,[1,2,3,4] Wenwen Cui,[1,*] Jingming Shi,[1] Artur P. Durajski,[5] Jian Hao,[1,†] Silvana Botti,[2,3,4,6,‡] Miguel A. L. Marques,[2,6,7,8] and Yinwei Li[1]

[1]*Laboratory of Quantum Functional Materials Design and Application, School of Physics and Electronic Engineering, Jiangsu Normal University, Xuzhou 221116, China*

[2]*Research Center Future Energy Materials and Systems of the Research Alliance Ruhr, D-44801 Bochum, Germany*

[3]*Faculty of Physics and Astronomy and ICAMS, Ruhr University Bochum, Universitätstrasse 150, D-44801 Bochum, Germany*

[4]*Institut für Festkörpertheorie und -optik, Friedrich-Schiller-Universität Jena, Max-Wien-Platz 1, 07743 Jena, Germany*

[5]*Institute of Physics, Częstochowa University of Technology, Ave. Armii Krajowej 19, 42-200 Częstochowa, Poland*

[6]*European Theoretical Spectroscopy Facility*

[7]*Institut für Physik, Martin-Luther-Universität Halle-Wittenberg, D-06099 Halle, Germany*

[8]*Faculty of Mechanical Engineering and ICAMS, Ruhr University Bochum, Universitätsstraße 150, D-44801 Bochum, Germany*

(Received 6 August 2023; revised 3 November 2023; accepted 21 November 2023; published 3 January 2024)

Hydrogen-rich superconductors are promising candidates to achieve room-temperature superconductivity. However, the extreme pressures needed to stabilize these structures significantly limit their practical applications. An effective strategy to reduce the external pressure is to add a light element M that binds with H to form MH_x units, acting as a chemical precompressor. We exemplify this idea by performing *ab initio* calculations of the Ac–Be–H phase diagram, proving that the metallization pressure of Ac–H binaries, for which critical temperatures as high as 200 K were predicted at 200 GPa, can be significantly reduced via beryllium incorporation. We identify three thermodynamically stable ($AcBe_2H_{10}$, $AcBeH_8$, and $AcBe_2H_{14}$) and four metastable compounds (fcc $AcBeH_8$, $AcBeH_{10}$, $AcBeH_{12}$ and $AcBe_2H_{16}$). All of them are superconductors. In particular, fcc $AcBeH_8$ remains dynamically stable down to 10 GPa, where it exhibits a superconducting-transition temperature T_c of 181 K. The Be–H bonds are responsible for the exceptional properties of these ternary compounds and allow them to remain dynamically stable close to ambient pressure. Our results suggest that high-T_c superconductivity in hydrides is achievable at low pressure and may stimulate experimental synthesis of ternary hydrides.

DOI: 10.1103/PhysRevB.109.014501

I. INTRODUCTION

The renaissance of high-T_c hydride superconductors began in 2004 [1,2] and has recently attracted growing attention, after a series of spectacular experimental confirmations, such as superconductivity at 200 K in SH_3 when subjected to an external pressure of 155 GPa [1–3], at 260 K and 170–180 GPa in LaH_{10} [4–8], at 215 K and 160 GPa or 172 GPa in CaH_6 [9–11], at 220 K and 166 GPa or 237 GPa in YH_6 [12–14], and at 243–262 K and 182–201 GPa in YH_9 [13,15]. Compared to pure hydrogen, the pressures required to realize metallization in binary hydrides are reduced considerably, but they are still so large to represent a serious limitation to any practical application. The search for high-T_c superconductors at lower or even ambient pressure remains an open challenge.

Thorough theoretical investigation of binary hydrides has revealed that most systems that display high-T_c (>150 K) superconductivity are stable only above 150 GPa [7,8,13,14], while those that could be stabilized at lower pressure exhibit poor superconductivity [16–19]. These relatively disappointing conclusions have however cleared the way for testing the largely unexplored family of ternary hydrides. In fact the additional chemical degree of freedom allows to enlarge enormously the search space, leading to exciting predictions with T_c close to the room temperature, such as Li_2MgH_{16} (T_c = 473 K at 250 GPa) [20], $YCeH_{20}$ (T_c = 246 K at 350 GPa), $LaCeH_{20}$ (T_c = 233 K at 250 GPa) [21], $(La,Y)H_{10}$ (T_c = 253 K at 183 GPa) [22], and $CaBeH_8$ (T_c = 254 K at 210 GPa) [23]. Encouragingly, several high-T_c ternary hydrides have already been experimentally synthesized, including $LaBeH_8$ (T_c = 110 K, at 80 GPa) [24], $(La,Ce)H_9$ (T_c = 48–172 K at 92–172 GPa) [25,26], $(La,Y)H_{10}$ (T_c = 253 K at 183 GPa) [22], and $(La, Nd)H_{10}$ (T_c = 148 K at 180 GPa) [27].

More specifically, we want to consider here the effect of adding a light element M that can bind with the H atoms to form small MH_x units. Such units can serve as precompression factor and act on the lattice of the parent binary to potentially reduce further the metallization pressure. For example, it was shown that introducing C atoms in a S-H system to obtain CH_4 molecules yields dynamically stable ternary compounds with good superconducting properties, comparable with those of SH_3 [28,29]. In particular, the work of Cataldo *et al.* on $LaBH_8$ (T_c = 126 K at 50 GPa) opened a new era of ternary superconducting hydrides with higher T_c in low-pressure environments [30]. Moreover, the incorporation of B or Be in lanthanum hydrides, forming Be/BH_8 units, makes this system dynamically stable down to below 50 GPa

*wenwencui@jsnu.edu.cn
†jian_hao@jsnu.edu.cn
‡silvana.botti@uni-jena.de

with a T_c above 100 K [23,30,31]. The formation of SiH_8 molecules with the same symmetry ensures the dynamical stability of $BaSiH_8$ and $SrSiH_8$ down to 3 GPa and 27 GPa, respectively [32]. Moreover, BH_4 molecules intercalating fcc lattices of alkaline metals X (X = K, Rb, Cs) lead to energetically stable, superconducting ternary hydrides XB_2H_8 with T_c above 100 K at 10 GPa [33,34].

Particularly interesting are the results obtained by incorporating Be atoms in binary hydrides: in fact, Be can act as electron donor to break the H_2 molecule and improve the superconducting properties, in the same way as Mg in Li_2MgH_{16} [20]. Moreover, it can lead to the formation of BeH_8 units that have the potential to reduce the metallization pressure of the parent hydride, as observed in $LaBeH_8$ (T_c = 183 K at 20 GPa) and $YBeH_8$ (T_c = 249 K at 100 GPa) [23]. The light Be atoms bind with H, replacing some H-H bonds in the hydrides, potentially leading to a reduction of the stabilization pressure. Additionally, doping with light elements can increase the average phonon frequencies, and if these vibrational modes are properly coupled with electrons at the Fermi energy (E_F), this can also contribute to an increase of T_c. Therefore, we consider very promising to insert Be atoms in high-T_c superconducting binary hydrides that are stable only at high pressures.

Actinium hydrides have been thoroughly studied at high pressures and several thermodynamically stable compounds have been proposed (e.g., AcH_2, AcH_3, Ac_3H_{10}, AcH_8, AcH_{10}, and AcH_{16}). Among these, AcH_{16} is predicted to be a good superconductor with T_c of 241 K at 150 GPa [35]. Here, we study the phase diagram of Ac–Be–H to find if the formation of BeH_x units can act as chemical precompressor of the fcc framework composed of the large Ac atoms, leading to ternary compounds that can be stable at low pressure. We perform therefore *ab initio* structural prediction calculations of $AcBe_xH_y$ (with $x = 1-2$, $y = 1-10$, 12, 14, 16, 18, 20) in search of thermodynamically stable and metastable structures that are metallic and potentially superconducting. Successive electron-phonon coupling (EPC) calculations are employed to evaluate the transition temperature for phonon-mediated superconductivity at different pressures.

We discover three stable phases $P1$ $AcBe_2H_{10}$, $Pmmn$ $AcBeH_8$, $Cmcm$ $AcBe_2H_{14}$ and four metastable phases $Fm\bar{3}m$ $AcBeH_8$, $Fm\bar{3}m$ $AcBeH_{10}$, $C2/m$ $AcBeH_{12}$, and $P4/mbm$ $AcBe_2H_{16}$. These structures are all dynamically stable, metallic, and superconducting. Our calculations predict that the $P4/mbm$ $AcBe_2H_{16}$ and $Fm\bar{3}m$ $AcBeH_{10}$ structures are superconductors with T_c of 150 K at 200 GPa and 165 K at 300 GPa, respectively. Particularly interesting is a metastable fcc structure of $AcBeH_8$ that remains dynamically stable down to 10 GPa with a high T_c of 181 K. Such a pressure is easy to achieve in an experiment, and is substantially lower than the required pressure to stabilize binary actinium hydrides.

II. COMPUTATIONAL DETAILS

The search for crystalline structures was performed using a particle-swarm optimization algorithm, as implemented in the CALYPSO code [37–40]. This method has been extremely successful in predicting stable and metastable superconducting hydrides [41], some of which have already been confirmed by experiments [28,42–45]. The calculations to predict the lowest enthalpy crystal structures of Ac_xBe_y binary system (with $x = 1-2$, $y = 1-6$) and of $AcBe_xH_y$ (with $x = 1-2$, $y = 1-10$, 12, 14, 16, 18, 20), considering up to four formula units, were done at 200 GPa. More than 2000 structures were sampled for each prediction run, for every composition, and each generation of structures was evolved by selecting the 60% lowest-enthalpy structures in the last step and randomly producing the remaining 40%. The structure searches were considered converged when ~1000 successive structures were generated without finding a new lowest-enthalpy structure. Structural relaxations and electronic band-structure calculations were performed using projector augmented-wave (PAW) method as implemented in the Vienna *Ab initio* Simulation Package (VASP) [46]. The exchange-correlation functional of density-functional theory was approximated by the generalized gradient approximation of Perdew, Burke, and Ernzerhof [47]. The ion-electron interaction was described by PAW potentials with $6s^26p^66d^17s^2$, $1s^22s^2$, and $1s^1$ electrons configurations as valence states for Ac, Be, and H atoms, respectively. In order to further test the reliability of the adopted PAW pseudopotentials under pressure, we compared the Birch-Murnaghan equation of state obtained with PAW potentials with the full-potential linearized augmented plane-wave method (LAPW), using local orbitals (as implemented in WIEN2k [48]). The results, in Fig. S1 of the Supplemental Material (SM) [49], fully validate our approach. The cutoff energy for the expansion of the wave functions in the plane wave basis was set to 1000 eV. Monkhorst-Pack k-point meshes [50] with a grid density of 0.20 $Å^{-1}$ were chosen to ensure a total energy convergence better than 1 meV per atom. The phonon spectrum and EPC were calculated within linear-response theory with the QUANTUM ESPRESSO code [51]. We define the EPC parameter

$$\lambda = 2\int_0^{\omega} \frac{\alpha^2 F(\omega)}{\omega} d\omega, \tag{1}$$

calculated from the $\alpha^2 F(\omega)$ is the Eliashberg spectral function and

$$\omega_{\log} = 2\int_0^{\omega} \frac{\alpha^2 F(\omega)}{\omega} ln(\omega) d\omega. \tag{2}$$

Ultrasoft pseudopotentials for Ac, Be, and H were used in EPC calculations [52]. The detailed encut, k meshes, and q points for these seven compounds can be found in Table S1 of the SM [49] for a Gaussian smearing width of 0.05 Ry. The convergence of the EPC parameter λ was tested using a set of Gaussian broadenings in steps of 0.001 Ry from 0.01 to 0.05 Ry with various k grids, as shown in Fig. S2 of the SM [49]. The superconducting critical temperature T_c is evaluated based on the Allen-Dynes-modified McMillan (ADM) equation [53] when the λ is smaller than 1.5:

$$T_c = \frac{\omega_{\log}}{1.2} \exp\left[-\frac{1.04(1+\lambda)}{\lambda - \mu^*(1+0.62\lambda)}\right], \tag{3}$$

and the corrected ADM by including two correction factors f_1 and f_2 to account for strong-coupling ($\lambda > 1.5$) and

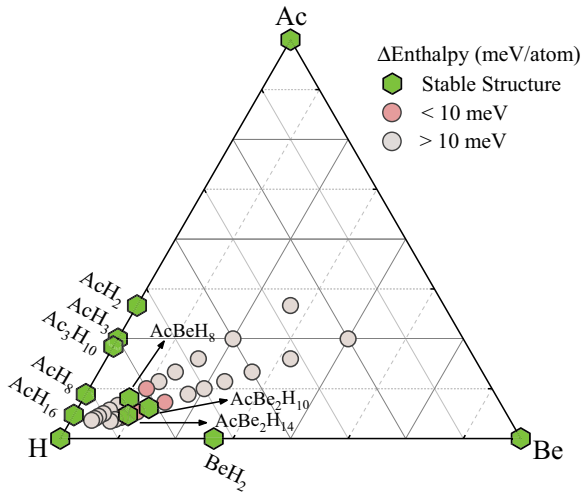

FIG. 1. Thermodynamical stability. Ternary convex hull of Ac–Be–H at 200 GPa. The stable and metastable phases are depicted as hexagons (green) and circles (pink and gray), respectively. Boundary binary phases of Ac–H [35] and Be–H [36] systems are chosen from the previous works and there is no stable structure in Ac–Be system, as shown in Fig. S3 [49]. We indicate in light red metastable structures that lie less than 10 meV/atom above the convex hull.

shape-correction multipliers, respectively:

$$T_c = f_1 f_2 \frac{\omega_{\log}}{1.2} \exp\left[\frac{-1.04(1+\lambda)}{\lambda - \mu^*(1+0.62\lambda)}\right]. \quad (4)$$

III. RESULTS AND DISCUSSION

We calculated the phase diagram of $AcBe_xH_y$ at 200 GPa (shown in Fig. 1) and found out that three ternary phases with stoichiometries $AcBe_2H_{10}$, $AcBeH_8$, and $AcBe_2H_{14}$ are stable against decomposition into elemental or binary solids. Additionally, we uncovered several metastable structures with distances to the convex hull smaller than around 10 meV/atom, namely, $AcBeH_6$ (9.3 meV/atom), $AcBe_2H_8$ (2.8 meV/atom), $AcBe_2H_{12}$ (2.4 meV/atom), $AcBe_2H_{16}$ (5.0 meV/atom), and $AcBeH_{12}$ (10.9 meV/atom). In view of the fact that hydrogen-rich phases with high symmetry have an increased potential to exhibit high-T_c superconductivity [6,54–58], we also consider two metastable phases with fcc symmetry $AcBeH_8$ (4 meV/atom) and $AcBeH_{10}$ (35 meV/atom). In particular, for the fcc $AcBeH_8$ phase, we compared relative enthalpies with respect to competing structures and possible decomposition products from 0 to 500 GPa, as shown in Figs. S4(a) and S4(b) [49]. In comparison to the work of Wan *et al.* [59], we performed prediction runs for several compositions of the Ac–Be–H phase diagram and not only for $XBeH_8$. Fig. S4(a) [49] indicates that the formation enthalpy of the fcc phase of $AcBeH_8$ is higher than the one of the thermodynamically stable *Pmmn* phase and of other metastable structures, as shown in Fig. S4(b) [49], but all the decomposition products exhibit positive formation energies relative to fcc $AcBeH_8$ above 30 GPa. The structure of $AcBeH_8$ with symmetry $Fm\bar{3}m$ is not thermodynamically stable in the range of pressures 0–30 GPa but our calculations suggest that there is a good possibility to synthesize this structure starting from $Ac_3H_{10} + BeH_2 + H_2$ below 200 GPa or at even lower pressure (30–50 GPa), through the synthesis paths $Ac_3H_{10} + Be + H_2$. As 10 GPa is an extremely low pressure, it is worth performing exploratory experiments. Other low-enthalpy structures may be accessible experimentally thanks to their small enthalpy distance to the convex hull at 200 GPa [5–8,22,60,61].

The crystal structures of thermodynamically stable and metastable $AcBe_xH_y$ compounds of 200 GPa are shown in Figs. 2 and S5 [49]. $AcBe_2H_{10}$ adopts a low-symmetry $P1$ structure [Fig. 2(a)] that contains BeH_8, BeH_7 units, and H_2 molecules, characterized by Be–H and H-H distances of 1.29–1.59 Å and 0.87 Å, respectively. The orthorhombic phase of $AcBeH_8$ [Fig. 2(b)] with space group *Pmmn* is composed of BeH_8 octahedra with a Be–H distance of 1.30–1.43 Å, as well as Ac atoms occupying the 2*a* Wyckoff positions. $AcBe_2H_{14}$ is also orthorhombic with *Cmcm* symmetry [Fig. 2(c)]. In this structure, Ac atoms occupying the 4*b* Wyckoff positions and three pairs of H_2 molecules, with bond lengths of around 0.85 Å, are positioned between pairs of Ac atoms. Additionally, two inequivalent Be atoms occupy the 4*a* and 4*c* Wyckoff positions. These Be atoms are surrounded by eight H atoms forming BeH_8 octahedra with Be–H distances of 1.36–1.56 Å at 200 GPa. In the metastable structure of $AcBe_2H_{16}$ with $P4/mbm$ symmetry [Fig. 2(d)], the Ac atoms occupy the 4*g* position: each Be is bonded with ten H atoms to form a hexadecahedal BeH_{10} unit. Adjacent BeH_{10} units along the *y* axis are connected with each other by sharing one hydrogen atom, and neighboring BeH_{10} units along the *c* axis are connected by dimers and trimers with H-H distances of 1.08 and 0.92 Å, respectively. The covalent nature of these latter bonds can be confirmed by analysis of the electron localization function (ELF), as shown in Fig. S6(a) [49]. The fcc phase of $AcBeH_8$ [Fig. 2(e)], isostructural to $Fm\bar{3}m$ $LaB(Be)H_8$ [23,24,30,31], consists of BeH_8 hexadra that occupy the octahedral sites of the fcc lattice formed by Ac atoms. The $AcBeH_{10}$ phase with $Fm\bar{3}m$ symmetry [Fig. 2(f)] is 15 meV/atom energetically higher than the lowest enthalpy phase $P2_1$. Compared with fcc $AcBeH_8$, the four additional H atoms of $AcBeH_{10}$ occupy tetrahedral sites that are connected by four BeH_8 octahedra to form H_5 regular tetrahedra with H-H distances of 1.00 Å. Other metastable structures (e.g., $P1$ $AcBeH_6$, $P\bar{1}$ $AcBe_2H_8$, *Cmmm* $AcBe_2H_{12}$, and $C2/m$ $AcBeH_{12}$) are shown in Fig. S5 [49]. In these structures, the Be and Ac atoms donate electrons to hydrogen, forming typical ionic hydrides (see Table SII [49]). Apart from the Be–H bonds, these metastable structures present also H-kagome lattices, together with dimers and trimers (see Fig. S5 [49]).

In order to further explore the fascinating properties of Ac–Be–H compounds, we calculated their electronic structure and phonon properties. Almost all predicted structures are also dynamically stable, as confirmed by inspection of the phonon bands, with the exception of $AcBe_2H_{12}$ and $AcBeH_{10}$ that display imaginary phonons (see Figs. 3 and S7 [49]). Even if $AcBe_2H_{12}$ and $AcBeH_{10}$ (Figs. S7(a) and S7(d) [49]) are not dynamically stable at 200 GPa, $AcBeH_{10}$ becomes stable at higher pressure [Fig. 3(f)]. The case of $Fm\bar{3}m$ $AcBeH_8$ is particularly interesting as it remains dynamically stable down to pressures of 10 GPa, as shown in Figs. 4(d) and S8 [49]. All considered structures are metallic with several bands crossing

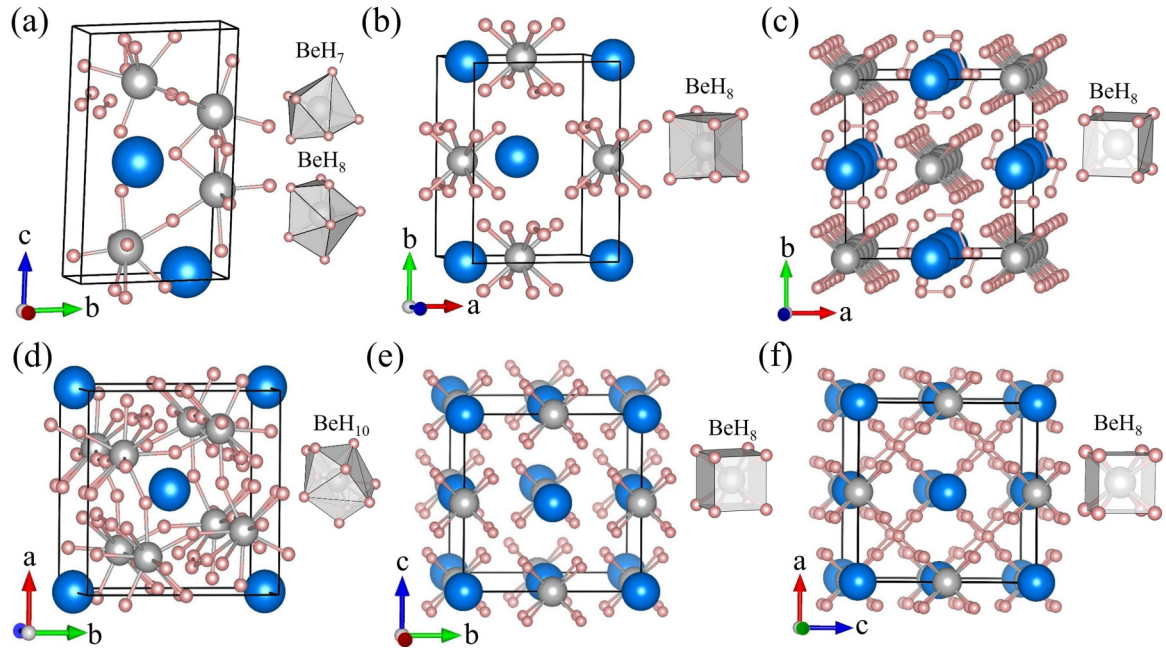

FIG. 2. Structural configuration. The stable (a)–(c) and metastable structures (d)–(f) of Ac–Be–H compounds. (a) $P1$ $AcBe_2H_{10}$, (b) $Pmmn$ $AcBeH_8$, (c) $Cmcm$ $AcBe_2H_{14}$, (d) $P4/mbm$ $AcBe_2H_{16}$, (e) $Fm\bar{3}m$ $AcBeH_8$, and (f) $Fm\bar{3}m$ $AcBeH_{10}$ at 200 GPa. Ac atoms are depicted in blue, Be in gray, and H in pink.

the Fermi energy E_F, and have therefore promising electronic bands for high-temperature superconductivity (see Figs. S9–S11 [49]). The significant overlap of the partial electronic density of states (DOS) of the different atoms indicates a strong hybridization of Ac–H and Be–H under pressure. The results clearly indicate that hydrogen atoms make a substantial contribution to the total DOS of E_F, e.g., for $Cmcm$ $AcBe_2H_{14}$ (49%), $P4/mbm$ $AcBe_2H_{16}$ (55%), $C2/m$ $AcBeH_{12}$ (49%), and $Fm\bar{3}m$ $AcBeH_8$ (44%) at 200 GPa (Table SIII [49]).

The contribution of hydrogen to the DOS at E_F (DOS_H) is large for the three stable structures $P1$ $AcBe_2H_{10}$, $Pmmn$ $AcBeH_8$, and $Cmcm$ $AcBe_2H_{14}$, with values 8.9×10^{-4}, 9.2×10^{-4}, and 6.8×10^{-4} states/(eV Å^3) at 200 GPa, respectively (Figs. S9(a)−S9(c)[49]). For the highly symmetric metastable structures, this contribution is even larger, especially in the case of $Fm\bar{3}m$ $AcBeH_8$, where we can observe an enhancement from 44% (200 GPa) to 65% (10 GPa). The corresponding hydrogen contributions to the DOS are 6.28×10^{-3} and 4.31×10^{-3} states/(eV Å^3), respectively. This enhances the coupling of the electrons to the H phonons, facilitating the formation of more Cooper pairs at E_F, and increasing the possibility of obtaining a higher superconducting transition temperature T_c (Figs. 4(a) and S10(a) [49]). There are three bands of fcc $AcBeH_8$ at 10 GPa that cross E_F, yielding the Fermi surface shown in Figs. 4(a) and 4(b). Bands 1 and 2 are degenerate along the high-symmetry line

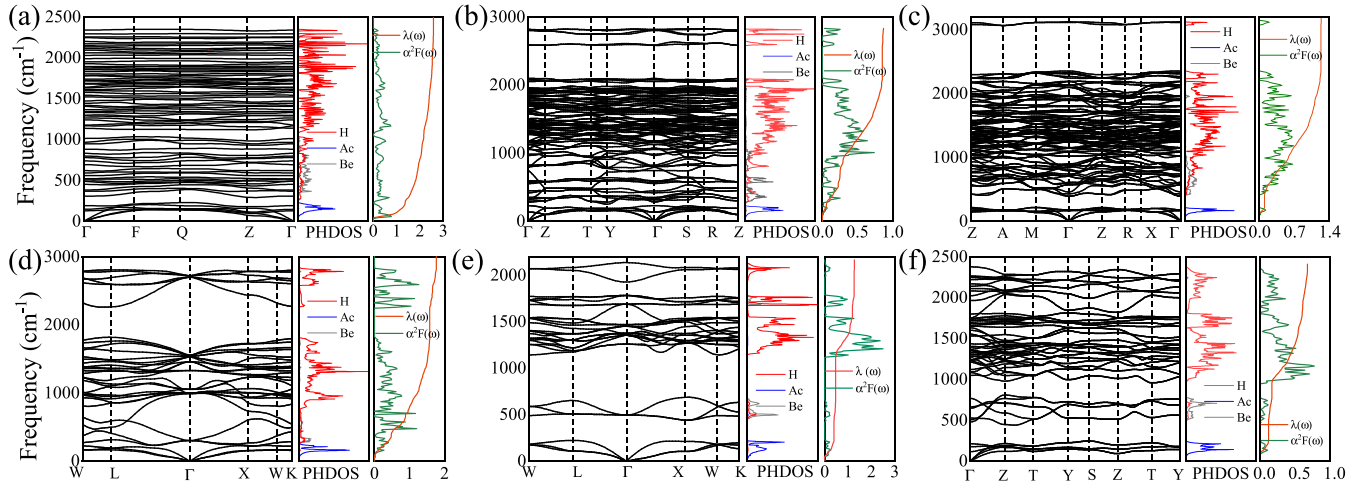

FIG. 3. Phonon band structures, phonon density of states (PHDOS), EPC coefficient $\lambda(\omega)$, and Eliashberg spectral function $\alpha^2F(\omega)$ of (a) $P1$ $AcBe_2H_{10}$, (b) $Pmmn$ $AcBeH_8$, (c) $Cmcm$ $AcBe_2H_{14}$, (d) $P4/mbm$ $AcBe_2H_{16}$, (e) $Fm\bar{3}m$ $AcBeH_8$, all at 200 GPa, and (f) $Fm\bar{3}m$ $AcBeH_{10}$ at 300 GPa.

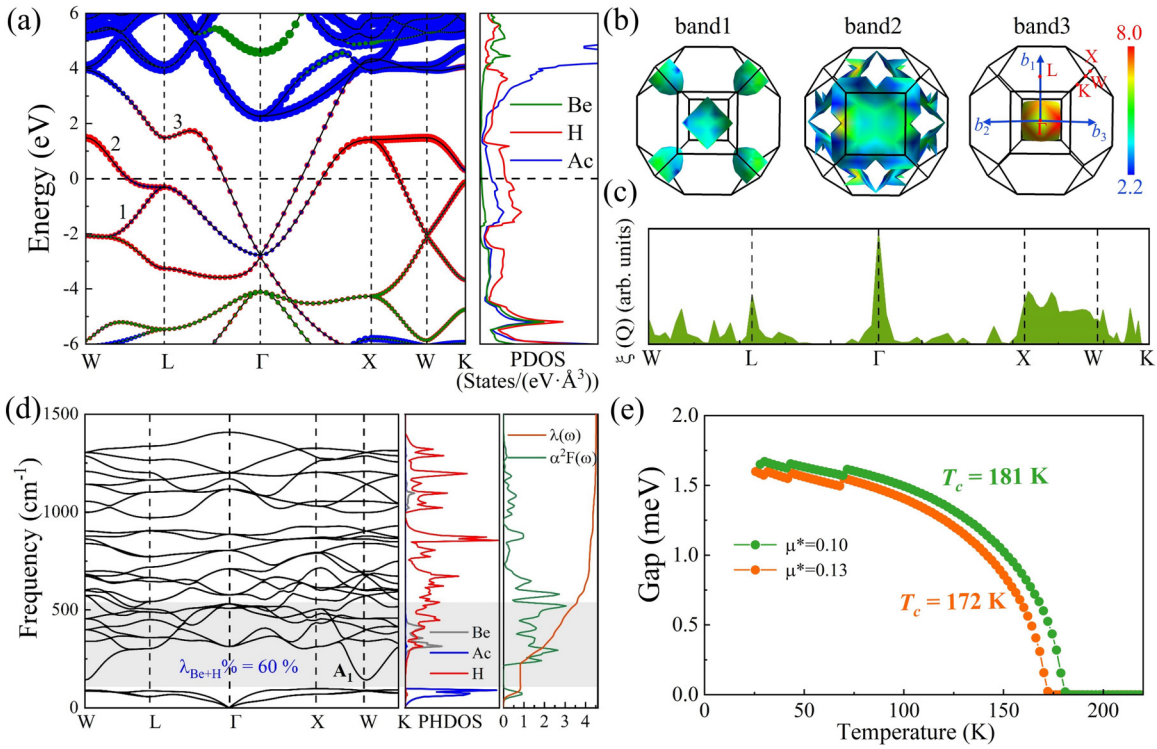

FIG. 4. Electronic and superconductivity properties of $AcBeH_8$ at 10 GPa. Calculated (a) band structures and projected density of states (PDOS), (b) Fermi surfaces corresponding to the three bands crossing the Fermi energy level, colored with respect to the Fermi velocity $\langle v \rangle$ (10^5 m/s), (c) nesting function $\xi(Q)$ along special Q trajectories, (d) phonon band structures, PHDOS, EPC coefficient $\lambda(\omega)$ and Eliashberg spectral function $\alpha^2F(\omega)$, and (e) isotropic superconducting gap of $Fm\bar{3}m$ $AcBeH_8$ at 10 GPa.

from L to X in the first Brillouin zone and their Fermi surface exhibits pockets at X and complex semiclosed shapes with a hexagonal opening at L. In addition to this, band 3 forms a closed electronlike surface at the Γ point, which leads to larger DOS at E_F and to a further enhancement of the EPC [62]. Despite the higher hydrogen content, the contribution of the H atoms to the DOS of $Fm\bar{3}m$ $AcBeH_{10}$ at E_F is less than that of $AcBeH_8$ (only 4.28×10^{-3} states/(eV Å^3) at 300 GPa, see Fig. S10(b) [49]). This is due to shift of about 2 eV of the bands around Fermi level, comparing with the bands of $AcBeH_{10}$ and $AcBeH_8$, we observe a shift of about 2 eV of a group of bands with strong H character close to the Fermi energy. This leads to a reduced H contribution to the DOS of E_F. More specifically, the H atoms in the same crystal graphic positions as in $AcBeH_8$ contribute now only 24% to the total DOS. The additional H atoms add only "a 15%" contribution. For other metastable structures with less symmetry (e.g., $P1$ $AcBeH_6$, $P\bar{1}$ $AcBe_2H_8$), the partial DOS of H at E_F amounts to less than $\sim 6.5 \times 10^{-4}$ states/(eV Å^3), which is not characteristic of superconductors with high critical temperature.

To investigate superconductivity and its mechanism, we calculated phonon dispersion curves, partial phonon density of states (PHDOS), the Eliashberg spectral function $\alpha^2F(\omega)$ and the EPC integrated $\lambda(\omega)$ of Ac–Be–H hydrides and we plotted these quantities in Figs. 3 and S8 [49]. The PHDOS of all structures has common features: the heaviest Ac atoms contribute to the lowest-frequency vibrational modes, the middle-frequency modes are mainly dominated by Be and H vibrations, and the high-frequency modes are exclusively due to H atoms.

The superconducting properties of the Ac–Be–H system can be estimated using the McMillan formula (as modified by Allen-Dynes [53]) or by solving numerically the Eliashberg equations [63]. We used the typical value of the Coulomb pseudopotential $\mu^* = 0.10$. A summary of the results can be found in Table I. Among the thermodynamically stable compounds, $AcBe_2H_{10}$ possesses the strongest EPC parameter $\lambda = 2.59$, mainly owing to the soft modes along the Z-Γ high-symmetry line [Fig. 3(a)], yielding a T_c of 115 K at

TABLE I. Superconducting-transition temperature. Logarithmic average phonon frequency (ω_{log}), EPC parameter λ, and T_c ($\mu^* = 0.10$) for $P1$ $AcBe_2H_{10}$, $Pmmn$ $AcBeH_8$, $Cmcm$ $AcBe_2H_{14}$, $P4/mbm$ $AcBe_2H_{16}$, $Fm\bar{3}m$ $AcBeH_8$, $C2/m$ $AcBe_2H_{12}$ at 200 GPa, and $Fm\bar{3}m$ $AcBeH_{10}$ at 300 GPa.

Compounds	λ	ω_{log} (K)	T_c (K) ADM	T_c (K) Eliashberg
$P1$ $AcBe_2H_{10}$	2.59	337	78	115
$Pmmn$ $AcBeH_8$	0.84	1262	66	75
$Cmcm$ $AcBe_2H_{14}$	0.67	1240	39	42
$P4/mbm$ $AcBe_2H_{16}$	1.19	1381	122	150
$Fm\bar{3}m$ $AcBeH_8$	1.32	724	73	118
$C2/m$ $AcBe_2H_{12}$	0.9	1130	66	78
$Fm\bar{3}m$ $AcBeH_{10}$	1.76	909	138	165

200 GPa. This is the highest T_c among the thermodynamically stable compounds. The low frequency region (0–245 cm^{-1}), dominated by the Ac atoms, contributes a significant amount (∼53%) to the total λ, but also the range of intermediate frequencies (245–1063 cm^{-1}), related to the Be–H bonds and the high-frequency region (1081–2358 cm^{-1}, due to H atoms only) contribute 30% and 17%, respectively, to λ, as shown in Table SIV [49]. The two other stable compounds *Pmmn* $AcBeH_8$ and *Cmcm* $AcBe_2H_{14}$ have values of λ of 0.67 and 0.84, respectively, at 200 GPa, and in both cases H atoms give the largest contribution to λ with 74% and 54%, respectively (Figs. 3(b)–3(c) and Table SIV [49]). The metastable structures $AcBe_2H_{16}$ and $AcBe_2H_{12}$ have values of λ of 1.19 and 0.9 at 200 GPa, yielding a T_c of 150 K and 78 K, respectively (see Table I).

In what concerns fcc $AcBeH_{10}$, we remark that it is not stable at 200 GPa (Fig. S7(a) [49]), but it is stabilized at the higher pressure of 300 GPa [Fig. 3(f)]. EPC calculations show that $Fm\bar{3}m$ $AcBeH_{10}$ phases are promising conventional superconductors with $\lambda = 1.76$ and $\omega_{log} = 909$ K at 300 GPa. This leads to an estimated T_c of 165 K. The phonon modes at frequencies between 427 and 2858 cm^{-1}, corresponding to vibrations of hydrogen atoms, contribute a large amount (72%) to the total λ (Tables I and SIV [49]).

The other fcc structure, $AcBeH_8$, is dynamically stable from 200 to 10 GPa, as shown by the phonon dispersion depicted in Figs. 3(e), S8 [49], and 4(d). The calculated λ and phonon frequency logarithmic average ω_{log} are 1.32 and 724 K at 200 GPa, respectively, leading to a T_c of 118 K for $\mu^* = 0.10$. Note that the vibrations related to H atoms at high frequencies give a significant contribution to the total λ (64–78%) for pressures in the range of 30–200 GPa, and the contribution of Be and H at intermediate frequencies only accounts for less than 6%. As the pressure decreases, λ increases proportionally to DOS_H, and the critical temperature of $AcBeH_8$ is gradually enhanced. λ increases from 1.32 to 2.3 from 200 to 100 GPa, and increases further from 2.3 to 4.5 from 100 GPa to 10 GPa, with T_c proportional to λ, as shown in Fig. 5. We conclude that $AcBeH_8$ is a typical superconductor dominated by λ. Strikingly, λ increases to 4.5 with a T_c of 181 K at 10 GPa (see Figs. 4(d)–4(e), 5, and Table SIV [49]). When the pressure decreases progressively to 10 GPa, the interaction between Be and H becomes stronger, and the contribution to λ due to soft phonon modes (110–540 cm^{-1}) increases to 60% ($\lambda_{Be}\% = 38\%$), especially thanks to contributions from the W point with symmetry C_{2v}, originating from A_1 modes that are mainly related to vibrations of hydrogen atoms (Figs. 4(d) and S12 [49]). There appears also a significant increase in the nesting function at 10 GPa along W-L and X-W-K, which is perfectly consistent with the phonon softening at W, as shown in Fig. 4(c). Our calculations indicate that under a pressure larger than 10 GPa, the main contribution to superconductivity comes from the H phonon modes, but down to very low pressure, the interaction between Be and H plays a key role in enhancing superconductivity while ensuring structural stability. This observation is surely relevant for future research of atmospheric-pressure high-temperature superconductors.

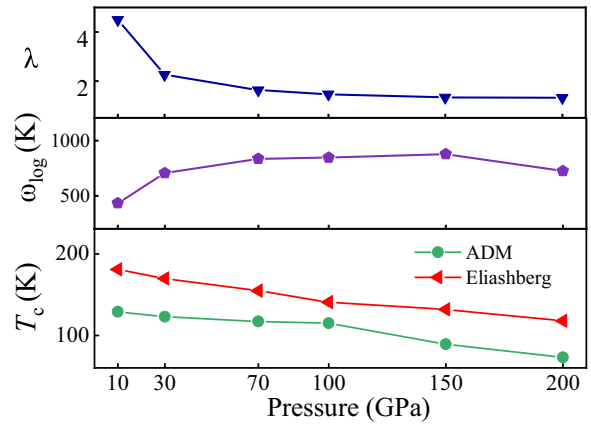

FIG. 5. Trend of calculated EPC parameters (λ), logarithmic average phonon frequency (ω_{log}), and the estimated T_c for selected structures using the Allen-Dynes modified McMillan (ADM) equation [53], and numerically solving the Eliashberg equations [63] with $\mu^* = 0.10$ for $Fm\bar{3}m$ $AcBeH_8$ at high pressures.

IV. CONCLUSIONS

In summary, we have investigated the crystal structures and superconductivity of stable and metastable ternary Ac–Be–H compounds, combining crystal structure prediction under pressure and first-principle calculations. At 200 GPa we uncover three thermodynamically stable compounds with stoichiometries $AcBe_2H_{10}$, $AcBeH_8$, $AcBe_2H_{14}$, as well as four metastable superconducting compounds, close to the convex hull: $AcBe_2H_{16}$, fcc $AcBeH_{10}$, fcc $AcBeH_8$ and $AcBe_2H_{12}$. All these structures exhibit metallic nature. Electron-phonon coupling calculations show that $AcBe_2H_{16}$ and fcc $AcBeH_{10}$ are good phonon-mediated superconductors with T_c of 150 K at 200 GPa and 165 K at 300 GPa, respectively. Very interestingly, fcc $AcBeH_8$ remains dynamically stable down to 10 GPa where it exhibits a T_c of 181 K. The soft phonon vibration modes originating from Be–H interactions in BeH_8 units contribute to the enhancement of superconductivity with decreasing pressure. We expect that our results will stimulate more research on ternary superconducting hydrides in the hope to uncover systems with high critical temperature and stability close to ambient pressure.

ACKNOWLEDGMENTS

The authors acknowledge funding from the NSFC under Grants No. 12074154, No. 11804128, No. 12174160, No. 11804129, and No. 11722433. W.C. and M.A.L.M. acknowledge the funding from the Sino-German Mobility Programme under Grant No. M-0362. Y.L. acknowledges the funding from the Six Talent Peaks Project and 333 High-level Talents Project of Jiangsu Province. K.G. acknowledges financial support from the China Scholarship Council. A.P.D. is grateful for financial support from the National Science Centre (Poland) through Project No. 2022/47/B/ST3/0062. All the calculations were performed at the High Performance Computing Center of the School of Physics and Electronic Engineering of Jiangsu Normal University.

[1] Y. Li, J. Hao, H. Liu, Y. Li, and Y. Ma, The metallization and superconductivity of dense hydrogen sulfide, J. Chem. Phys. **140**, 174712 (2014).

[2] D. Duan, Y. Liu, F. Tian, D. Li, X. Huang, Z. Zhao, H. Yu, B. Liu, W. Tian, and T. Cui, Pressure-induced metallization of dense $(H_2S)_2H_2$ with high-T_c superconductivity, Sci. Rep. **4**, 6968 (2014).

[3] A. Drozdov, M. Eremets, I. Troyan, V. Ksenofontov, and S. I. Shylin, Conventional superconductivity at 203 kelvin at high pressures in the sulfur hydride system, Nature (London) **525**, 73 (2015).

[4] H. Liu, I. I. Naumov, R. Hoffmann, N. Ashcroft, and R. J. Hemley, Potential high-T_c superconducting lanthanum and yttrium hydrides at high pressure, Proc. Natl. Acad. Sci. **114**, 6990 (2017).

[5] M. Kostrzewa, K. Szczęśniak, A. Durajski, and R. Szczęśniak, From LaH_{10} to room–temperature superconductors, Sci. Rep. **10**, 1592 (2020).

[6] F. Peng, Y. Sun, C. J. Pickard, R. J. Needs, Q. Wu, and Y. Ma, Hydrogen clathrate structures in rare earth hydrides at high pressures: possible route to room-temperature superconductivity, Phys. Rev. Lett. **119**, 107001 (2017).

[7] A. Drozdov, P. Kong, V. Minkov, S. Besedin, M. Kuzovnikov, S. Mozaffari, L. Balicas, F. Balakirev, D. Graf, V. Prakapenka *et al.*, Superconductivity at 250 K in lanthanum hydride under high pressures, Nature (London) **569**, 528 (2019).

[8] M. Somayazulu, M. Ahart, A. K. Mishra, Z. M. Geballe, M. Baldini, Y. Meng, V. V. Struzhkin, and R. J. Hemley, Evidence for superconductivity above 260 K in lanthanum superhydride at megabar pressures, Phys. Rev. Lett. **122**, 027001 (2019).

[9] H. Wang, S. T. John, K. Tanaka, T. Iitaka, and Y. Ma, Superconductive sodalite-like clathrate calcium hydride at high pressures, Proc. Natl. Acad. Sci. **109**, 6463 (2012).

[10] L. Ma, K. Wang, Y. Xie, X. Yang, Y. Wang, M. Zhou, H. Liu, X. Yu, Y. Zhao, H. Wang *et al.*, High-temperature superconducting phase in clathrate calcium hydride CaH_6 up to 215 K at a pressure of 172 GPa, Phys. Rev. Lett. **128**, 167001 (2022).

[11] Z. Li, X. He, C. Zhang, X. Wang, S. Zhang, Y. Jia, S. Feng, K. Lu, J. Zhao, J. Zhang *et al.*, Superconductivity above 200 K discovered in superhydrides of calcium, Nat. Commun. **13**, 2863 (2022).

[12] Y. Li, J. Hao, H. Liu, J. S. Tse, Y. Wang, and Y. Ma, Pressure-stabilized superconductive yttrium hydrides, Sci. Rep. **5**, 9948 (2015).

[13] P. Kong, V. S. Minkov, M. A. Kuzovnikov, A. P. Drozdov, S. P. Besedin, S. Mozaffari, L. Balicas, F. F. Balakirev, V. B. Prakapenka, S. Chariton *et al.*, Superconductivity up to 243 K in the yttrium-hydrogen system under high pressure, Nat. Commun. **12**, 5075 (2021).

[14] I. A. Troyan, D. V. Semenok, A. G. Kvashnin, A. V. Sadakov, O. A. Sobolevskiy, V. M. Pudalov, A. G. Ivanova, V. B. Prakapenka, E. Greenberg, A. G. Gavriliuk *et al.*, Anomalous high-temperature superconductivity in YH_6, Adv. Mater. **33**, 2006832 (2021).

[15] E. Snider, N. Dasenbrock-Gammon, R. McBride, X. Wang, N. Meyers, K. V. Lawler, E. Zurek, A. Salamat, and R. P. Dias, Synthesis of yttrium superhydride superconductor with a transition temperature up to 262 K by catalytic hydrogenation at high pressures, Phys. Rev. Lett. **126**, 117003 (2021).

[16] K. Shimizu, H. Ishikawa, D. Takao, T. Yagi, and K. Amaya, Superconductivity in compressed lithium at 20 K, Nature (London) **419**, 597 (2002).

[17] N. Wang, P. Shan, K. Chen, J. Sun, P. Yang, X. Ma, B. Wang, X. Yu, S. Zhang, G. Chen *et al.*, A low-T_c superconducting modification of Th_4H_{15} synthesized under high pressure, Supercond. Sci. Technol. **34**, 034006 (2021).

[18] M. Dietrich, W. Gey, H. Rietschel, and C. Satterthwaite, Pressure dependence of the superconducting transition temperature of Th_4H_{15}, Solid State Commun. **15**, 941 (1974).

[19] J. Schirber and C. Northrup Jr., Concentration dependence of the superconducting transition temperature in PdH_x and PdD_x, Phys. Rev. B **10**, 3818 (1974).

[20] Y. Sun, J. Lv, Y. Xie, H. Liu, and Y. Ma, Route to a superconducting phase above room temperature in electron-doped hydride compounds under high pressure, Phys. Rev. Lett. **123**, 097001 (2019).

[21] P. Song, Z. Hou, K. Nakano, K. Hongo, and R. Maezono, Potential high-T_c superconductivity in $YCeH_x$ and $LaCeH_x$ under pressure, Mater. Today Phys. **28**, 100873 (2022).

[22] D. V. Semenok, I. A. Troyan, A. G. Ivanova, A. G. Kvashnin, I. A. Kruglov, M. Hanfland, A. V. Sadakov, O. A. Sobolevskiy, K. S. Pervakov, I. S. Lyubutin *et al.*, Superconductivity at 253 K in lanthanum–yttrium ternary hydrides, Mater. Today **48**, 18 (2021).

[23] Z. Zhang, T. Cui, M. J. Hutcheon, A. M. Shipley, H. Song, M. Du, V. Z. Kresin, D. Duan, C. J. Pickard, and Y. Yao, Design principles for high-temperature superconductors with a hydrogen-based alloy backbone at moderate pressure, Phys. Rev. Lett. **128**, 047001 (2022).

[24] Y. Song, J. Bi, Y. Nakamoto, K. Shimizu, H. Liu, B. Zou, G. Liu, H. Wang, and Y. Ma, Stoichiometric ternary superhydride $LaBeH_8$ as a new template for high-temperature superconductivity at 110 K under 80 GPa, Phys. Rev. Lett. **130**, 266001 (2023).

[25] J. Bi, Y. Nakamoto, P. Zhang, K. Shimizu, B. Zou, H. Liu, M. Zhou, G. Liu, H. Wang, and Y. Ma, Giant enhancement of superconducting critical temperature in substitutional alloy $(La,Ce)H_9$, Nat. Commun. **13**, 5952 (2022).

[26] W. Chen, X. Huang, D. V. Semenok, S. Chen, D. Zhou, K. Zhang, A. R. Oganov, and T. Cui, Enhancement of superconducting properties in the La–Ce–H system at moderate pressures, Nat. Commun. **14**, 2660 (2023).

[27] D. V. Semenok, I. A. Troyan, A. V. Sadakov, D. Zhou, M. Galasso, A. G. Kvashnin, A. G. Ivanova, I. A. Kruglov, A. A. Bykov, K. Y. Terent'ev *et al.*, Effect of magnetic impurities on superconductivity in LaH_{10}, Adv. Mater. **34**, 2204038 (2022).

[28] W. Cui, T. Bi, J. Shi, Y. Li, H. Liu, E. Zurek, and R. J. Hemley, Route to high-T_c superconductivity via CH_4-intercalated H_3S hydride perovskites, Phys. Rev. B **101**, 134504 (2020).

[29] Y. Sun, Y. Tian, B. Jiang, X. Li, H. Li, T. Iitaka, X. Zhong, and Y. Xie, Computational discovery of a dynamically stable cubic SH_3-like high-temperature superconductor at 100 GPa via CH_4 intercalation, Phys. Rev. B **101**, 174102 (2020).

[30] S. Di Cataldo, C. Heil, W. von der Linden, and L. Boeri, $LaBH_8$: Towards high-T_c low-pressure superconductivity in ternary superhydrides, Phys. Rev. B **104**, L020511 (2021).

[31] X. Liang, A. Bergara, X. Wei, X. Song, L. Wang, R. Sun, H. Liu, R. J. Hemley, L. Wang, G. Gao *et al.*, Prediction of

high-T_c superconductivity in ternary lanthanum borohydrides, Phys. Rev. B **104**, 134501 (2021).
[32] R. Lucrezi, S. Di Cataldo, W. von der Linden, L. Boeri, and C. Heil, In-silico synthesis of lowest-pressure high-T_c ternary superhydrides, npj Comput. Mater. **8**, 119 (2022).
[33] S. Li, H. Wang, W. Sun, C. Lu, and F. Peng, Superconductivity in compressed ternary alkaline boron hydrides, Phys. Rev. B **105**, 224107 (2022).
[34] M. Gao, X.-W. Yan, Z.-Y. Lu, and T. Xiang, Phonon-mediated high-temperature superconductivity in the ternary borohydride KB_2H_8 under pressure near 12 GPa, Phys. Rev. B **104**, L100504 (2021).
[35] D. V. Semenok, A. G. Kvashnin, I. A. Kruglov, and A. R. Oganov, Actinium hydrides AcH_{10}, AcH_{12}, and AcH_{16} as high-temperature conventional superconductors, J. Phys. Chem. Lett. **9**, 1920 (2018).
[36] S. Yu, Q. Zeng, A. R. Oganov, C. Hu, G. Frapper, and L. Zhang, Exploration of stable compounds, crystal structures, and superconductivity in the Be-H system, AIP Adv. **4**, 107118 (2014).
[37] Y. Wang, J. Lv, L. Zhu, and Y. Ma, Crystal structure prediction via particle-swarm optimization, Phys. Rev. B **82**, 094116 (2010).
[38] Y. Wang, J. Lv, L. Zhu, and Y. Ma, Calypso: A method for crystal structure prediction, Comput. Phys. Commun. **183**, 2063 (2012).
[39] B. Gao, P. Gao, S. Lu, J. Lv, Y. Wang, and Y. Ma, Interface structure prediction via calypso method, Sci. Bull. **64**, 301 (2019).
[40] X. Shao, J. Lv, P. Liu, S. Shao, P. Gao, H. Liu, Y. Wang, and Y. Ma, A symmetry-orientated divide-and-conquer method for crystal structure prediction, J. Chem. Phys. **156**, 014105 (2022).
[41] W. Cui and Y. Li, The role of calypso in the discovery of high-T_c hydrogen-rich superconductors, Chin. Phys. B **28**, 107104 (2019).
[42] J. A. Flores-Livas, L. Boeri, A. Sanna, G. Profeta, R. Arita, and M. Eremets, A perspective on conventional high-temperature superconductors at high pressure: Methods and materials, Phys. Rep. **856**, 1 (2020).
[43] E. Zurek and T. Bi, High-temperature superconductivity in alkaline and rare earth polyhydrides at high pressure: A theoretical perspective, J. Chem. Phys. **150**, 050901 (2019).
[44] J. Ma, J. Kuang, W. Cui, J. Chen, K. Gao, J. Hao, J. Shi, and Y. Li, Metal-element-incorporation induced superconducting hydrogen clathrate structure at high pressure, Chin. Phys. Lett. **38**, 027401 (2021).
[45] J. Shi, W. Cui, J. Hao, M. Xu, X. Wang, and Y. Li, Formation of ammonia–helium compounds at high pressure, Nat. Commun. **11**, 1 (2020).
[46] G. Kresse and J. Furthmüller, Efficient iterative schemes for *ab initio* total-energy calculations using a plane-wave basis set, Phys. Rev. B **54**, 11169 (1996).
[47] J. P. Perdew, K. Burke, and M. Ernzerhof, Generalized gradient approximation made simple, Phys. Rev. Lett. **77**, 3865 (1996).
[48] P. Blaha, K. Schwarz, P. Sorantin, and S. Trickey, Full-potential, linearized augmented plane wave programs for crystalline systems, Comput. Phys. Commun. **59**, 399 (1990).
[49] See Supplemental Material at http://link.aps.org/supplemental/10.1103/PhysRevB.109.014501 for testing the accuracy of the PAW pseudopotentials, and the convergence of k meshes, respectively, 2D convex hull of the binary Ac-Be system at 200 GPa, structural information, average charge transfer in one unit cell of Ac-Be-H compounds; the phonon-dispersion curves, PHDOS, $\alpha^2F(\omega)$, Eliashberg spectral function for other compounds, electronic band structures and projected density of states (PDOS) and contribution to the density of states (DOS) of H, Be, and Ac atoms, etc.
[50] W. Tang, E. Sanville, and G. Henkelman, A grid-based bader analysis algorithm without lattice bias, J. Phys.: Condens. Matter **21**, 084204 (2009).
[51] P. Giannozzi, S. Baroni, N. Bonini, M. Calandra, R. Car, C. Cavazzoni, D. Ceresoli, G. L. Chiarotti, M. Cococcioni, I. Dabo *et al.*, Quantum espresso: a modular and open-source software project for quantum simulations of materials, J. Phys.: Condens. Matter **21**, 395502 (2009).
[52] G. Kresse and D. Joubert, From ultrasoft pseudopotentials to the projector augmented-wave method, Phys. Rev. B **59**, 1758 (1999).
[53] P. B. Allen and R. Dynes, Transition temperature of strong-coupled superconductors reanalyzed, Phys. Rev. B **12**, 905 (1975).
[54] H. Xie, Y. Yao, X. Feng, D. Duan, H. Song, Z. Zhang, S. Jiang, S. A. T. Redfern, V. Z. Kresin, C. J. Pickard, and T. Cui, Hydrogen pentagraphenelike structure stabilized by hafnium: A high-temperature conventional superconductor, Phys. Rev. Lett. **125**, 217001 (2020).
[55] M. Du, H. Song, Z. Zhang, D. Duan, and T. Cui, Room-temperature superconductivity in heavy rare earth metal substituted sodalite-lie clathrate hexahydrides under moderate pressure, arXiv:2204.11043.
[56] Y. Sun, S. Sun, X. Zhong, and H. Liu, Prediction for high superconducting ternary hydrides below megabar pressure, J. Phys.: Condens. Matter **34**, 505404 (2022).
[57] Y. Hou, B. Li, Y. Bai, X. Hao, Y. Yang, F. Chi, S. Liu, J. Cheng, and Z. Shi, Superconductivity in $CeBeH_8$ and $CeBH_8$ at moderate pressures, J. Phys.: Condens. Matter **34**, 505403 (2022).
[58] Q. Jiang, Z. Zhang, H. Song, Y. Ma, Y. Sun, M. Miao, T. Cui, and D. Duan, Ternary superconducting hydrides stabilized via Th and Ce elements at mild pressures, Fundam. Res. (2022), doi: 10.1016/j.fmre.2022.11.010.
[59] Z. Wan, T. Yang, W. Xu, and R. Zhang, Superconductivity and magnetism in compressed actinium-beryllium-hydrogen alloys, arXiv:2209.01903.
[60] W. Chen, D. V. Semenok, X. Huang, H. Shu, X. Li, D. Duan, T. Cui, and A. R. Oganov, High-temperature superconducting phases in cerium superhydride with a T_c up to 115 K below a pressure of 1 Megabar, Phys. Rev. Lett. **127**, 117001 (2021).
[61] N. P. Salke, M. M. Davari Esfahani, Y. Zhang, I. A. Kruglov, J. Zhou, Y. Wang, E. Greenberg, V. B. Prakapenka, J. Liu, A. R. Oganov *et al.*, Synthesis of clathrate cerium superhydride CeH_9 at 80-100 GPa with atomic hydrogen sublattice, Nat. Commun. **10**, 4453 (2019).
[62] A. Simon, Superconductivity and chemistry, Angew. Chem., Int. Ed. Engl. **36**, 1788 (1997).
[63] G. M. Eliashberg, Interactions between electrons and lattice vibrations in a superconductor, JETP **11**, 696 (1960).